Express Polymer Letters Vol.18, No.6 (2024) 575–591
Available online at www.expresspolymlett.com
https://doi.org/10.3144/expresspolymlett.2024.43

Research article

Electrospun organically modified sepiolite/PVDF coating on polypropylene separator to improve electrochemical performance of lithium-ion battery

Xianli Sun[1,2], *Jiahao Xu*[1,2], *Xiaoke Zhi*[3], *Jingpeng Zhang*[4], *Kangwei Hou*[1,2], *Yuhan Bian*[1,2], *Xiaolin Li*[1,2], *Li Wang*[1,2,5*], *Guangchuan Liang*[1,2,5]

[1]School of Materials Science and Engineering, Hebei University of Technology, 300130 Tianjin, China
[2]Key Laboratory of Special Functional Materials for Ecological Environment and Information (Hebei University of Technology), Ministry of Education, 300130 Tianjin China
[3]School of Energy and Chemical Engineering, Tianjin Renai College, 301636 Tianjin, China
[4]Shandong Goldencell Electronics Technology Co., Ltd., Zaozhuang, 277021 Shandong, China
[5]Functional Lithium Ion Battery Materials Engineering Research Center of Jiangxi Province, Xinyu, 338019 Jiangxi, China

Received 31 January 2024; accepted in revised form 9 March 2024

Abstract. As a key component of lithium-ion batteries, a separator with excellent electrolyte wettability and good thermal stability has an important impact on the overall performance of lithium-ion batteries. Herein, a PVDF/sepiolite electrospun layer was coated on one side of the PP separator via electrospinning technology to prepare the composite separator (xMS-PVDF@PP) with sepiolite nanofibers modified with vinyltriethoxysilane (VTES) to ameliorate their dispersibility and compatibility with PVDF polymer matrix. The effect of modified sepiolite addition amounts on the physical and electrochemical properties of composite separator was intensively studied. It is found that the as-prepared xMS-PVDF@PP composite separator displays enhanced porosity, electrolyte uptake, thermal stability and Li^+ ion transport kinetics than pristine PP separator. Specifically, Li|$LiFePO_4$ battery with 20MS-PVDF@PP as separator shows the best rate and cycling performance, with a specific discharge capacity of 115.3 $mAh·g^{-1}$ at 10C rate and a capacity retention rate of 97.06% after 200 cycles at 1C rate. The sepiolite in the electrospun layer can immobilize PF_6^- anion to facilitate the uniform distribution of Li^+ ions and then inhibit the lithium dendrite growth, as well as absorb HF to alleviate Fe^{2+} dissolution from $LiFePO_4$ cathode, thereby further improving the electrochemical performance of $LiFePO_4$ battery.

Keywords: *lithium-ion battery, separator, sepiolite, electrospinning technology*

1. Introduction

Currently, lithium-ion batteries (LIB) are widely utilized in various mobile electronic devices, electric vehicles, energy storage systems, and other fields [1–3]. As an inseparable and important part of LIB, the separator has two main functions. One is to separate the positive and negative electrodes to prevent a short circuit of the battery. The other is to allow the passage of Li^+ ions and anions but electronic insulation [4, 5]. The performance of separators significantly influences the electrochemical performance and safety of LIB. Currently, polyolefin-based separators, such as polypropylene (PP) and polyethylene (PE), have been widely used in commercial LIB due to low cost, proper electrochemical stability and mechanical strength [6]. However, there also exist some shortcomings of poor electrolyte wettability and thermal stability [7, 8]. In addition, the poor interface compatibility between the polyolefin separator and lithium anode easily leads to the growth of lithium

---

[*] Corresponding author, e-mail: wangli_hebut@163.com

dendrites, thereby adversely affecting the safety and electrochemical performance of LIB [9].

Among various modification methods, organic polymer coating has attracted more attentions to improve the shortcomings of polyolefin separators. Compared with PP and PE, poly(vinylidene fluoride) (PVDF) polymer has a higher affinity with electrolytes and higher thermal and electrochemical stability [10, 11] thereby its coating on polyolefin-based separator can achieve better electrolyte wettability and thermal stability. However, directly coating PVDF on a polyolefin-based separator may block some pores and affect the ionic conductivity. Electrospinning is a method of preparing nanofiber separators with high specific surface area and porosity. The resulting separators can absorb a large amount of electrolyte and provide effective transport channels, thus endowing the separator with higher electrolyte uptake and ionic conductivity [12]. However, the electrospun separator usually has poor mechanical strength. And this defect can be remedied by electrospinning on the surface of polyolefin-based separator to prepare an electrospun coating, which endows the obtained composite separator with the advantages of both electrospun separator and polyolefin-based separator.

However, PVDF still has serious thermal shrinkage at high temperatures, which prevents its wide application in LIB. Recently, some inorganic minerals as fillers have been added to polymers to increase thermal stability. Natural clay has been commonly used as inorganic fillers, given its unique characteristics [13, 14]. Sepiolite is a fibrous hydrated magnesium silicate clay mineral with a large specific surface area, excellent adsorption capability, and a large amount of silanol (–SiOH) group. As an inorganic filler, it can simultaneously improve the thermal stability and electrolyte wettability of polymer separator. Deng *et al*. [15] used electrospinning technology to prepare a PU/sepiolite composite separator, which showed good thermal stability and high ionic conductivity. Guo *et al*. [16] used electrospinning technology to prepare a PVDF/sepiolite coating on a PP surface, and the as-prepared composite separator not only inherited the advantages of the PP separator but also improved the electrolyte uptake and thermal shrinkage of the separator. Zhang *et al*. [17] used an organic-inorganic (PVA-PIB) composite binder to coat sepiolite on both sides of the PE separator, which improved the porosity, electrolyte absorption, ionic conductivity and thermal stability of the separator. However, due to the high surface energy of sepiolite fiber, it is difficult to disperse uniformly in the polymer, which affects the performance of the separator. Therefore, it is necessary to modify the sepiolite first to improve its dispersibility and compatibility with the polymer matrix.

Vinyltriethoxysilane (VTES, $CH_2{=}CHSi(OC_2H_5)_3$) is a silane coupling agent with ideal properties, where $–Si(OC_2H_5)_3$ can be hydrolyzed under certain conditions to bond with hydroxyl group (–OH) on inorganic substance to ameliorate the agglomeration of inorganic substance in organic matrix, and the organic functional group in VTES molecule is well compatible with organic matrix. Therefore, in this work, VTES is adopted to organically modify sepiolite fibers to improve their dispersibility and compatibility with PVDF polymer matrix. However, the hydrolysis process of VTES is very slow under neutral conditions, thereby an appropriate amount of ammonia was added to accelerate the hydrolysis of VTES. The OH^- from ammonia could attack the Si atom on VTES and cause the ethoxy group ($–OC_2H_5$) to fall off. In this way, VTES is transformed into silanol and undergoes dehydration condensation with the hydroxyl group on sepiolite to achieve the successful graft of VTES onto sepiolite.

Herein, electrospinning technology was adopted to prepare a PVDF electrospun layer incorporated with VTES-modified sepiolite as filler on the surface of the PP separator. On the one hand, the presence of PVDF can enhance the electrolyte wettability of the separator. On the other hand, the sepiolite nanofibers modified by VTES can improve their dispersion and compatibility in the PVDF polymer matrix. The Lewis acid on the sepiolite can immobilize PF_6^- anions, which can further facilitate the transport of Li^+ ions. In addition, the adsorption characteristics of sepiolite itself can adsorb HF generated in the electrolyte to inhibit the relevant side reactions. The effect of different amounts of modified sepiolite on the physical and electrochemical properties of composite separators was systematically studied.

2. Experimental

2.1. Sample synthesis

2.1.1. Sepiolite treatment

The modification process of sepiolite by VTES (AR, purity 97%, Macklin, Shanghai, China) is as follows. Sepiolite powder (CP, Xiangtan Sepiolite Technology

Co., Hunan, China) was acid-leached to remove impurities in advance, labelled as Sep.

0.25 g Sep powder was added to 20 mL absolute ethanol (AR, purity 99.5%, Macklin, Shanghai, China) and ultrasonically treated for 15 min to obtain Sep suspension. 2.5 g VTES was added to 15 mL absolute ethanol and stirred for 30 min, which was then added dropwise to above Sep suspension. An appropriate amount of ammonia (AR, 25 wt% concentration, Sinopharm, Shanghai, China) was added to adjust pH = 10. The mixed suspension was heated to 80 °C and reacted for 2.5 h. The obtained product was washed with absolute ethanol and filtered three times. Finally, it was dried at 80 °C for 12 h to obtain the modified sepiolite, named as M-Sep.

2.1.2. Preparation of composite separator

Initially, a certain amount of PVDF (AR, Average M_w ~1 100 000, Macklin, Shanghai, China) was dissolved in *N*,*N*-dimethylformamide (DMF, AR, purity 99%, Macklin, Shanghai, China) to prepare a PVDF/DMF solution with concentration of 9 wt%, which was magnetically stirred for 3 h at room temperature to ensure complete dissolution of PVDF. Then, different amounts of M-Sep (10, 20, 30, 40 wt% based on PVDF) were added to four PVDF/DMF solutions. The mixture was stirred overnight to obtain a uniform spinning solution and left to stand for additional 1 h to remove bubbles from the solution. PP separator (Celgard 2500, Battery Grade, thickness 25 μm, Celgard Company, North Carolina, USA) was used as the base and wound on the collector. The spinning solution was transferred to a syringe and installed on the electrospinning machine (DP30, Yunfan Technology, Tianjin, China) for single-sided electrospinning. The spinning parameters were set as voltage of 14 kV, feed rate of 0.0012 mm·s^{-1}, and rotation speed of 150 rpm. Finally, the obtained separator was dried in a vacuum oven at 80 °C for 12 h to remove residual solvent. The composite separator was then pressed using a roller machine (MSK-2150, Shenzhen Kejing, Shenzhen, China) to control the thickness to ~32 μm. The resulting composite separators with M-Sep amounts of 10, 20, 30, 40 wt% were named as 10MS-PVDF@PP, 20MS-PVDF@PP, 30MS-PVDF@PP, and 40MS-PVDF@PP, respectively. For comparison, a PVDF layer without M-Sep powder was also electrospun on the surface of PP separator through the same procedure, and the resulting composite separator was called PVDF@PP.

2.2. Sample characterization

The changes in chemical bonds and functional groups of sepiolite and electrospun coatings were characterized using Fourier Transform Infrared Spectroscopy (FT-IR, V80, Bruker Corporation, Bruker, Germany) in the range of 4000-400 cm^{-1} with a resolution of 4 cm^{-1}. The morphologies of sepiolite and electrospun coatings were observed by scanning electron microscopy (SEM, Hitachi S-4800, Hitachi, Ltd., Tokyo, Japan). The crystal structure of sepiolite was examined by X-ray diffractometer (XRD, D8 FOCUS, Bruker Corporation, Bruker, Germany) with Cu K_α radiation (λ = 0.15406 nm) in 2θ range of 6–80° at a sweep rate of 6°·min^{-1}.

Electrolyte wettability of the separator was tested by dipping 20 μL liquid electrolyte (Battery Grade, Huzhou Kunlun Yienke Battery Materials Co. Ltd, Huzhou, China) on the surface of separator, and a photograph was taken after 2 s.

The porosity of separator was calculated based on the weight of the separator before and after soaked in *n*-butanol (AR, purity 99%, Fuchen, Tianjin, China) for 2 h using the Equation (1):

$$\mathit{Porosity}\,[\%] = \frac{M_1 - M_0}{\rho V}\cdot 100 \qquad (1)$$

where M_0 and M_1 are the weight of the separator before and after soaked in *n*-butanol, respectively, ρ is the density of *n*-butanol, and V is the volume of separator.

Electrolyte uptake was calculated based on the weight of the separator before and after soaked in liquid electrolyte for 2 h using Equation (2):

$$\mathit{Electrolyte\ uptake}\,[\%] = \frac{W_1 - W_0}{W_0}\cdot 100 \qquad (2)$$

where W_0 and W_1 are the weight of the separator before and after soaked in liquid electrolyte, respectively.

The thermal stability of PP and composite separators was studied by placing them in an oven at 140 °C for 30 min and then their dimensional change was observed by digital camera.

Ionic conductivity was measured using AC impedance spectroscopy with an amplitude of 10 mV and a frequency range of 10^{-2}–10^5 Hz on SS|separator|SS blocking cells by assembling the separator between two stainless steel (SS) electrodes, and calculated according to Equation (3):

$$\sigma = \frac{l}{R_\mathrm{b}A} \tag{3}$$

where σ is the ionic conductivity [$\mathrm{S{\cdot}cm^{-1}}$], R_b is the bulk resistance of electrolyte, l and A are the thickness and effective area of separator, respectively.

The electrochemical stability of separator was studied by linear sweep voltammetry (LSV) using Li|separator|SS cells in the voltage range of 3–6 V at a scan rate of 10 $\mathrm{mV{\cdot}s^{-1}}$ on CHI660E electrochemical workstation (Shanghai Chenhua Instrument Co. Ltd, Shanghai, China).

Li^+ ions transfer number (t_{Li^+}) of the separator was measured by the combination of chronoamperometry and AC impedance spectroscopy on Li||Li symmetric cells, and calculated according to Equation (4):

$$t_{\mathrm{Li}^+} = \frac{I_\mathrm{S}(\Delta V - I_0R_0)}{I_0(\Delta V - I_\mathrm{S}R_\mathrm{S})} \tag{4}$$

where R_0 and R_S are the interfacial resistance before and after polarization obtained from EIS, respectively; I_0 and I_S are the initial current and the steady-state current obtained from chronoamperometry after polarization, and ΔV is the step potential difference (10 mV).

2.3. Electrochemical test

$LiFePO_4$ cathode was composed of $LiFePO_4$ active material (Battery Grade, Shandong Goldencell Electronics Technology Co., Ltd, Zaozhuang, China), Super P (Battery Grade, Kolud, Shanghai, China), and PVDF in a weight ratio of 8:1:1. The electrolyte-soaked separator was placed between $LiFePO_4$ cathode and lithium anode in an Ar-filled glove box (Lab2000, Etelux, Beijing, China) to assemble CR2430 coin cell, with the electrospun layer facing lithium anode. Rate capability and cycling performance were evaluated on LAND CT2001A battery testing system (Wuhan LAND Electronic Co. Ltd, Wuhan, China). Electrochemical impedance spectroscopy (EIS) tests were conducted in a two-electrode system on an electrochemical workstation with lithium metal as counter and reference electrode.

3. Results and discussion

3.1. Structure and morphology

Figure 1a shows the XRD patterns of Sep and M-Sep powders. The diffraction peaks of Sep match well with the standard card (JCPDS#75-1597) of sepiolite. The major diffraction peaks at 2θ = 7.3°, 11.8°, 20.6° and 26.5° correspond to (110), (130), (131) and (400) crystal planes of sepiolite, respectively. Besides, the peak at 2θ =9.451° corresponds to the main diffraction peak of talc, implying the presence of tiny amount of talc impurity in Sep sample. After modification with VTES, the diffraction pattern of M-Sep remains almost unchanged, suggesting the unchanged crystalline structure of Sep. Figure 1b shows the XRD patterns of PP and 20MS-PVDF@PP separators. The main diffraction peak of sepiolite at 2θ = 7.3° can be observed in the XRD pattern of 20MS-PVDF@PP separator, confirming the successful introduction of sepiolite on PP separator. The relatively lower peak intensity may be ascribed to the low content and the encapsulation of M-Sep within PVDF matrix.

Figure 1c shows FT-IR spectra of pristine sepiolite (Sep) and VTES-modified sepiolite (M-Sep). It can be seen that in both spectra, the peaks in the range of 1300–900 $\mathrm{cm^{-1}}$ are attributed to symmetric and asymmetric vibrations related to Si–O–Si and Si–O [18], the peaks at 3613 and 3555 $\mathrm{cm^{-1}}$ are attributed to the stretching vibration of hydroxyl group from Mg–OH [19], and the peak at 785 $\mathrm{cm^{-1}}$ corresponds to the bending vibration of Mg–OH [20]. Besides, the peak at 3387 $\mathrm{cm^{-1}}$ is assigned to zeolite water in sepiolite [21], and that at 1658 $\mathrm{cm^{-1}}$ corresponds to the symmetric and asymmetric stretching vibrations of crystalline water and zeolite water [18, 22]. The M-Sep sample shows all characteristic peaks related to sepiolite. Besides, we also observe that compared to Sep, M-Sep exhibits two stretching vibration peaks at 2900 and 2980 $\mathrm{cm^{-1}}$ related to the C–H bond from $-CH_3$ and $-CH_2-$ of unhydrolyzed $-OC_2H_5$ group of VTES [23, 24], as shown in the magnified spectra in Figure 1d, indicating the successful graft of VTES onto sepiolite. VTES modification makes sepiolite organophilic, thus leading to its better compatibility with the PVDF matrix.

Figures 1e shows SEM images of Sep and M-Sep samples. Both Sep and M-Sep exhibit needle-like nanofiber structures. For the Sep sample, a large number of sepiolite nanofibers are staggered and agglomerated together due to the high surface energy of sepiolite nanofibers. However, the modification with VTES can reduce the surface energy of sepiolite nanofibers, thus leading to the more uniform dispersion of sepiolite nanofibers without agglomeration. The well-dispersed sepiolite nanofibers are

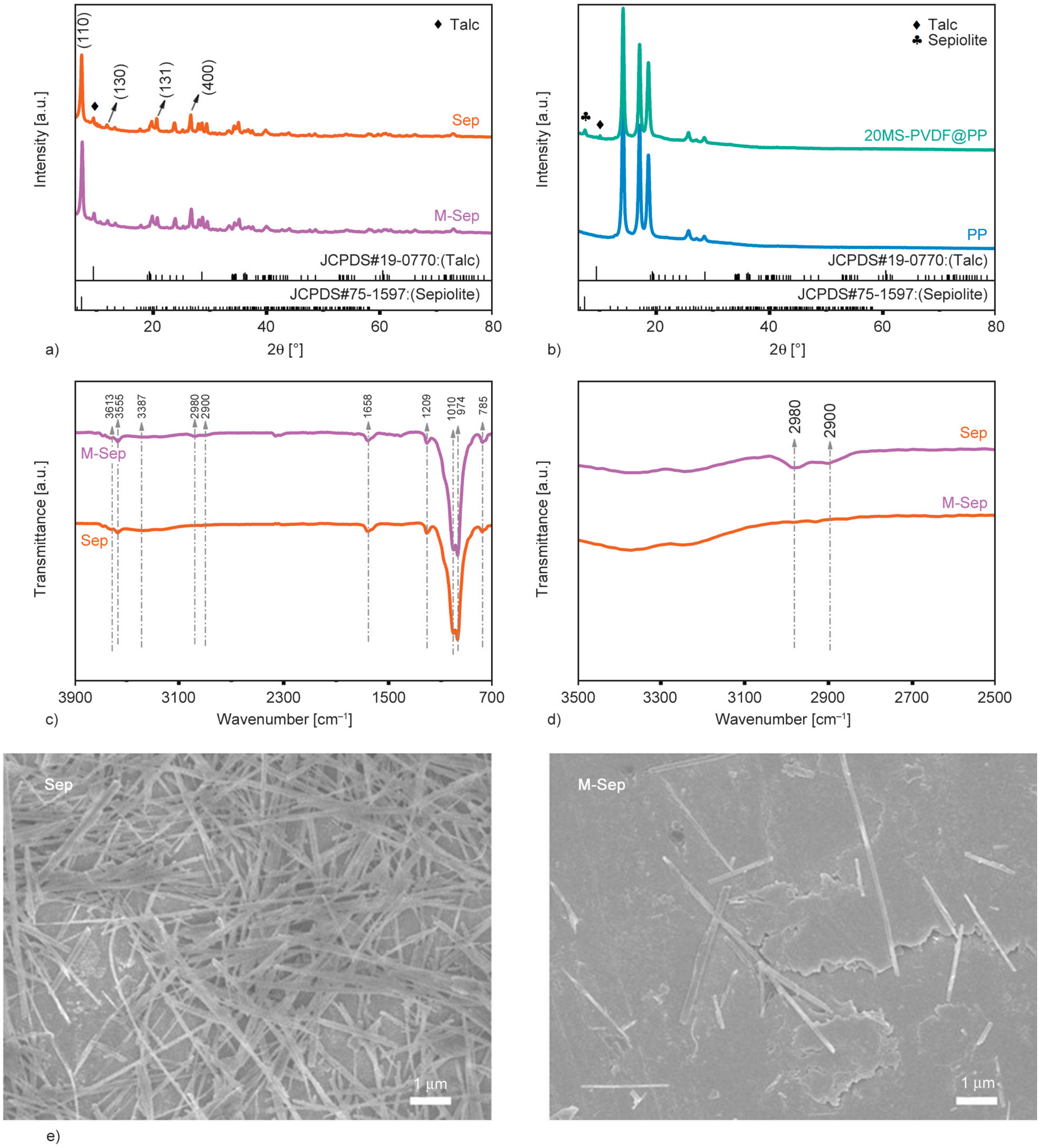

Figure 1. XRD patterns of Sep and M-Sep (a), XRD patterns of PP and 20MS-PVDF@PP (b), FT-IR spectra (c) and magnified spectra between 3500 and 2500 cm^{-1} (d) for Sep and M-Sep, and SEM images for Sep and M-Sep (e).

beneficial to the electrolyte uptake of the separator, thereby improving the physical and electrochemical properties of the separator.

Figure 2a shows FT-IR spectra of PVDF coatings without and with modified sepiolite. The absorption peaks at 3020, 2980 cm^{-1} (stretching vibration of C–H), 1400 cm^{-1} (bending vibration of C–H), 1178 cm^{-1} (stretching vibration of C–F), and 840 cm^{-1} (swinging vibration of $–CH_2–$) can be ascribed to PVDF [25, 26]. The absorption peak of Si–O–Si in the range of 900–1100 cm^{-1} and that of Mg–OH in the range of 3550–3600 cm^{-1} (in Figure 2b) suggest the inclusion of sepiolite in PVDF coating. It can be clearly observed that the intensity of the Si–O–Si-related absorption peak increases gradually with the M-Sep addition amount.

Figure 3 shows SEM images of PVDF electrospun layers without and with different amounts of M-Sep and corresponding fiber diameter distribution histograms. It is obvious that all electrospun coatings

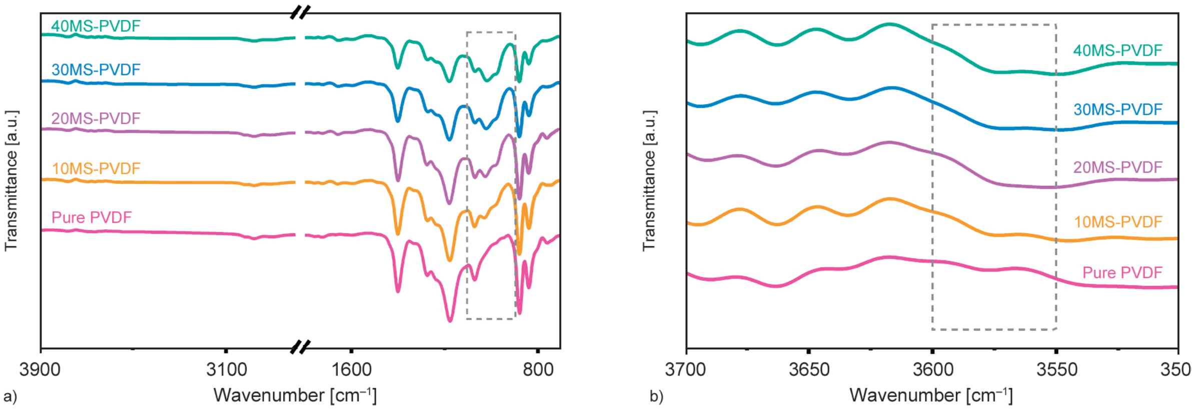

Figure 2. FT-IR spectra (a) and magnified spectra between 3700 and 3500 cm^{-1} (b) for PVDF layers before and after incorporation of M-Sep.

exhibit a 3D network structure formed by randomly stacked nanofibers, which guarantees a porous structure with high porosity, facilitating the migration of Li^+ ions and electrolyte uptake. Compared with pure PVDF fiber in Figure 3a, the fibers with M-Sep addition display a relatively rougher surface. As the addition amount of M-Sep increases, the surface of fibers becomes rougher gradually. In addition, from Figure 3c–3e, we can observe the attachment of sepiolite on the surface of fibers, confirming the presence of sepiolite in the composite separator. On the other hand, it can be clearly observed that the fiber diameter gradually increases with the M-Sep amount, which is induced by the higher viscosity of the spinning solution after the addition of more M-Sep powders. In addition, from the histograms in the insets of Figure 3a–3e, it can be seen that with the amount of M-Sep increasing from 0 to 20 wt%, the distribution of fiber diameter becomes gradually uniform. This is because, with the increase of M-Sep content, the viscosity of the spinning solution increases gradually. Under the action of electrostatic field, the fibers can be fully stretched and the filament production becomes more stable. Moreover, the addition of M-Sep powder improves the stiffness of fibers; thereby, the resulting fibers display a gradually smaller diameter and more uniform distribution with M-Sep addition. On the other hand, excessive addition of M-Sep to 30 and 40 wt% results in reduced distribution uniformity. More seriously, after the addition of 40 wt% M-Sep powder, the sepiolite nanofibers agglomerate seriously, and some large nodules appear on the surface of the electrospun fiber, as shown in Figure 3e. This is because excessive M-Sep addition may increase the viscosity of the spinning solution greatly. During the electrospinning process, under the action of the electrostatic field, insufficient stretching of nanofibers easily leads to the agglomeration of sepiolite and then the formation of some large nodules, thereby blocking some pores and reducing the porosity, which adversely affects the migration of Li^+ ions and electrochemical performance of the separator. Figure 3f shows the element mapping images of Si, Mg and F for the 20MS-PVDF@PP separator. From the uniform distribution of Si and Mg elements, it can be inferred that the sepiolite nanofibers are uniformly distributed in the electrospun PVDF layer.

3.2. Physical properties

Electrolyte wettability can reflect the migration of Li^+ ions, which directly affects the electrochemical performance of the battery. Figure 4a shows the electrolyte wettability test of PP and 20MS-PVDF@PP separators. After 20 μL electrolyte was dipped on the separator surface, the electrolyte remained in a spherical shape on the PP surface, demonstrating its poor electrolyte wettability due to its inherent hydrophobicity and low surface energy [27]. However, the electrolyte immediately loses dimensional stability and is completely absorbed by a 20MS-PVDF@PP separator, exhibiting its excellent electrolyte wettability, which is primarily linked to higher porosity and better electrolyte affinity of 20MS-PVDF electrospun layer and good hydrophilicity of sepiolite nanofibers. The excellent electrolyte wettability of 20MS-PVDF@PP is expected to enhance the rate capability and cycling performance of batteries. On the one hand, good electrolyte wettability of separator is beneficial to Li^+ ions transport by providing sufficient channels, which can enhance the ionic conductivity of separator and reduce the electrochemical

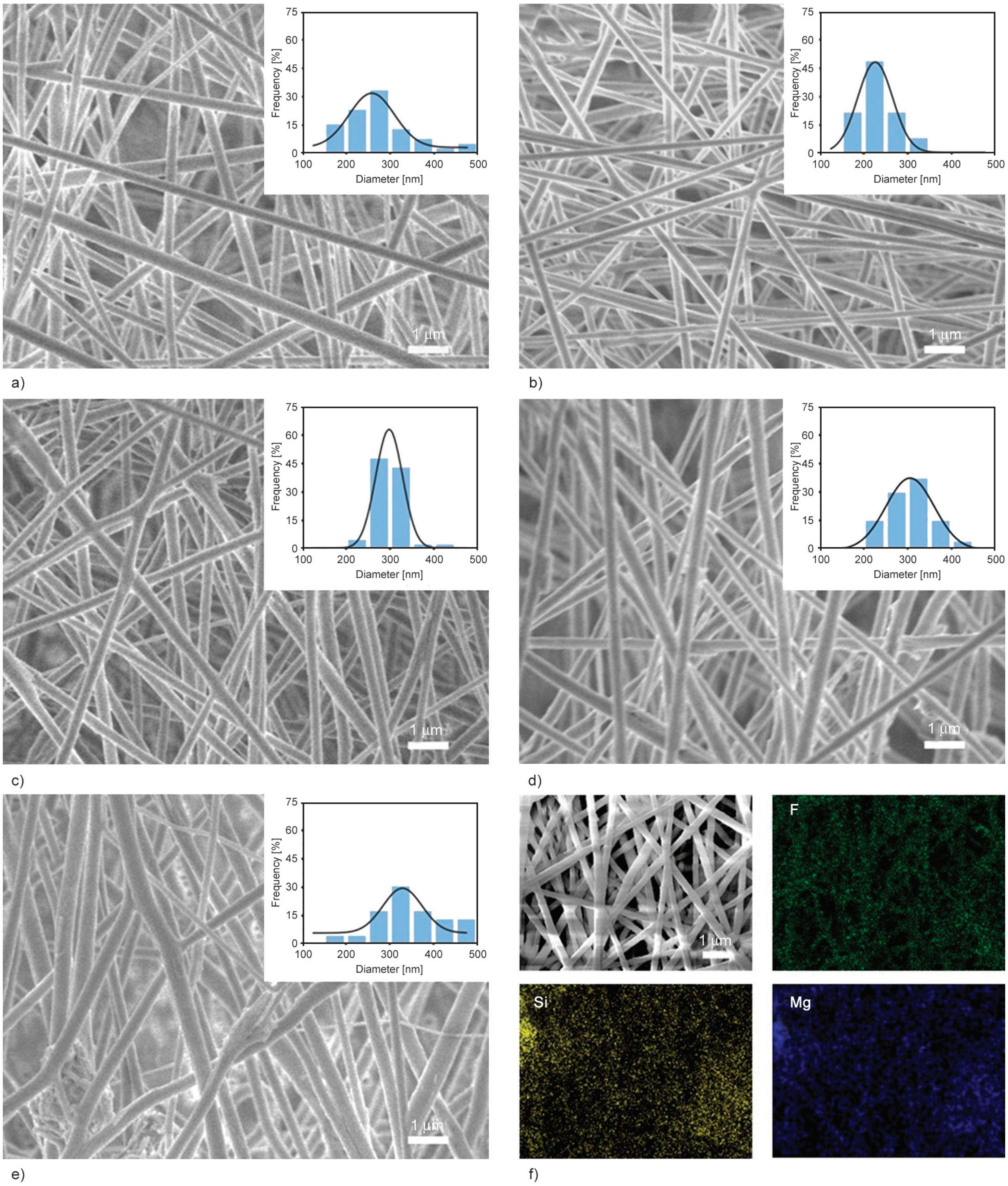

Figure 3. SEM images and histograms of fiber diameter distribution of PVDF@PP (a), 10MS-PVDF@PP (b), 20MS-PVDF@PP (c), 30MS-PVDF@PP (d), 40MS-PVDF@PP (e) and element mapping images of 20MS-PVDF@PP (f).

polarization during charge/discharge process, thus improving the rate capability of battery. On the other hand, good electrolyte wettability is conductive to the uniform distribution of Li^+ ions flux, which can prevent Li^+ ions locally concentrated, thereby suppressing the formation of lithium dendrite on lithium anode surface, thus improving the cycle stability of battery.

Porosity is an important parameter for porous separators because it greatly influences the electrochemical performance of LIB. Table 1 lists the porosity of PP and composite separators. Since the PP separator

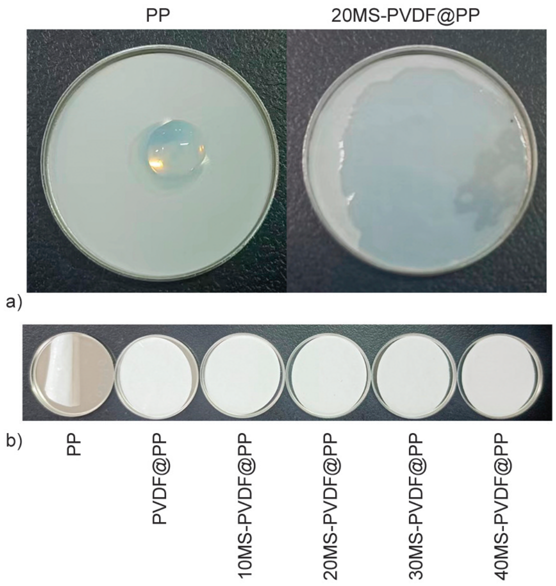

Figure 4. Wettability test (a) and thermal stability test (b) for PP and composite separators.

is usually prepared by dry or wet process, its porosity is generally as low as 40%. Due to the presence of porous electrospun coating, the porosity of PVDF@PP and xMS-PVDF@PP composite separators is enhanced obviously compared with PP. As the M-Sep amount increases from 0 to 20 wt%, the porosity of composite separators gradually increases to a maximum of 62% for the 20MS-PVDF@PP separator. This is mainly attributed to the porous network structure, which has a more concentrated distribution of fiber diameter. However, with the further increase of the M-Sep addition amount, the porosity of the composite separator decreases contrarily, which is only 43% for the 40MS-PVDF@PP separator. This is because excessive M-Sep results in the higher viscosity of the spinning solution, which results in the increased fiber diameter with nonuniform distribution and even the appearance of some nodules in the electrospun fibers of 40MS-PVDF@PP, which may block some micropores of PP substrate to a greater extent, thus leading to lower porosity than 20MS-PVDF@PP. The phenomenon illustrates that excessive M-Sep addition leads to poor spinning properties of spinning solution, affects the uniformity and structure of electrospun fibers, and then the porosity of composite separator.

Table 1. Porosity and electrolyte uptake rate of PP and composite separators.

Separator	Porosity [%]	Electrolyte uptake [%]
PP	40	249
PVDF@PP	45	511
10MS-PVDF@PP	57	614
20MS-PVDF@PP	62	653
30MS-PVDF@PP	51	547
40MS-PVDF@PP	43	484

The electrolyte uptake is also an important indicator of separator, which is closely related to porosity. From Table 1, it can be seen that the composite separator has significantly higher electrolyte uptake than the PP separator (249%), which is 511, 614, 653, 547 and 484% for PVDF@PP, 10MS-PVDF@PP, 20MS-PVDF@PP, 30MS-PVDF@PP and 40MS-PVDF@PP, respectively. That is to say, its variation rule with the M-Sep addition amount is in accordance with that of porosity. The enhanced electrolyte uptake is mainly ascribed to the following reasons. Firstly, the higher porosity of composite separator is conductive to electrolyte uptake. Secondly, the hydrophilicity and high specific surface area of M-Sep are also beneficial to electrolyte uptake. Thirdly, the introduction of M-Sep destroys the orderly arrangement of macromolecular chains and increases the proportion of amorphous regions in PVDF matrix, thereby further promoting the electrolyte uptake [27]. However, excessive M-Sep addition leads to larger fiber diameter, nonuniform fiber diameter distribution and lower porosity, thus leading to lower electrolyte uptake for the 40MS-PVDF@PP separator. Higher porosity and electrolyte uptake are believed to be advantageous to the rapid migration of Li^+ ions, thereby enhancing the rate capability and cycling performance of the battery. On the one hand, higher porosity and electrolyte uptake can provide more channels for the migration of Li^+ ions, thus accelerating the migration of Li^+ ions and then reducing the electrochemical polarization of the battery, which ultimately improves the rate performance of the battery. On the other hand, higher porosity and electrolyte uptake can make Li^+ ions flux more uniform and reduce the formation of lithium dendrites, which is conducive to the cycling performance of the battery.

High thermal stability is an essential requirement for separators, which enables them to maintain their dimensions even at high temperatures due to short circuits caused by overcharging [28]. Figure 4b shows the photos of different separators after being placed in an oven at 140 °C for 30 min. It can be observed that the PP separator exhibits serious shrinkage, while PVDF@PP and xMS-PVDF@PP separators basically maintain their initial dimensions, indicating the PVDF coating with incorporation of M-Sep can improve the thermal stability of the PP separator. This can be partly attributed to the higher melting point of PVDF and sepiolite. On the other hand, the sepiolite nanofibers can act as a 'crosslinking agent' to retard the motion of polymer chains, thus enhancing the thermal stability of the polymer [29]. It is accepted that higher temperatures may induce higher mobility of polymer chains, which leads to easier shrinkage of the polymer and worse thermal stability. However, the addition of sepiolite can hinder the motion of polymer chains and then enhance the temperature at which the polymer shrinks, thereby improving the thermal stability of the composite separator.

Figure 5a shows the AC impedance spectra of SS|separator|SS block cells using PP and composite separators. The bulk resistance (R_b) of separator can be obtained from the intercept in high-frequency region, and the ionic conductivity calculated according to Equation (3) is shown in Figure 5b. Compared to PP separator with a low ionic conductivity of 0.33 mS·cm^{-1}, the composite separators exhibit higher ionic conductivities, which is mainly related to the porous structure and better electrolyte wettability. For xMS-PVDF@PP separators, as M-Sep addition amount increases from 0 to 20 wt%, the ionic conductivity increases from 0.56 to 0.98 mS·cm^{-1}, which can be attributed to the increment in porosity and electrolyte wettability by the addition of M-Sep. In addition, the introduction of M-Sep to the PVDF polymer matrix increases the amorphous region of the polymer, which is also conducive to ionic conductivity [30]. However, as the M-Sep addition amount further increases, the larger electrospun fiber diameter with nonuniform distribution, along with the appearance of some large nodules, lead to the decreased porosity and electrolyte uptake and, ultimately, a decreased ionic conductivity of 0.50 mS·cm^{-1} for 40MS-PVDF@PP separator.

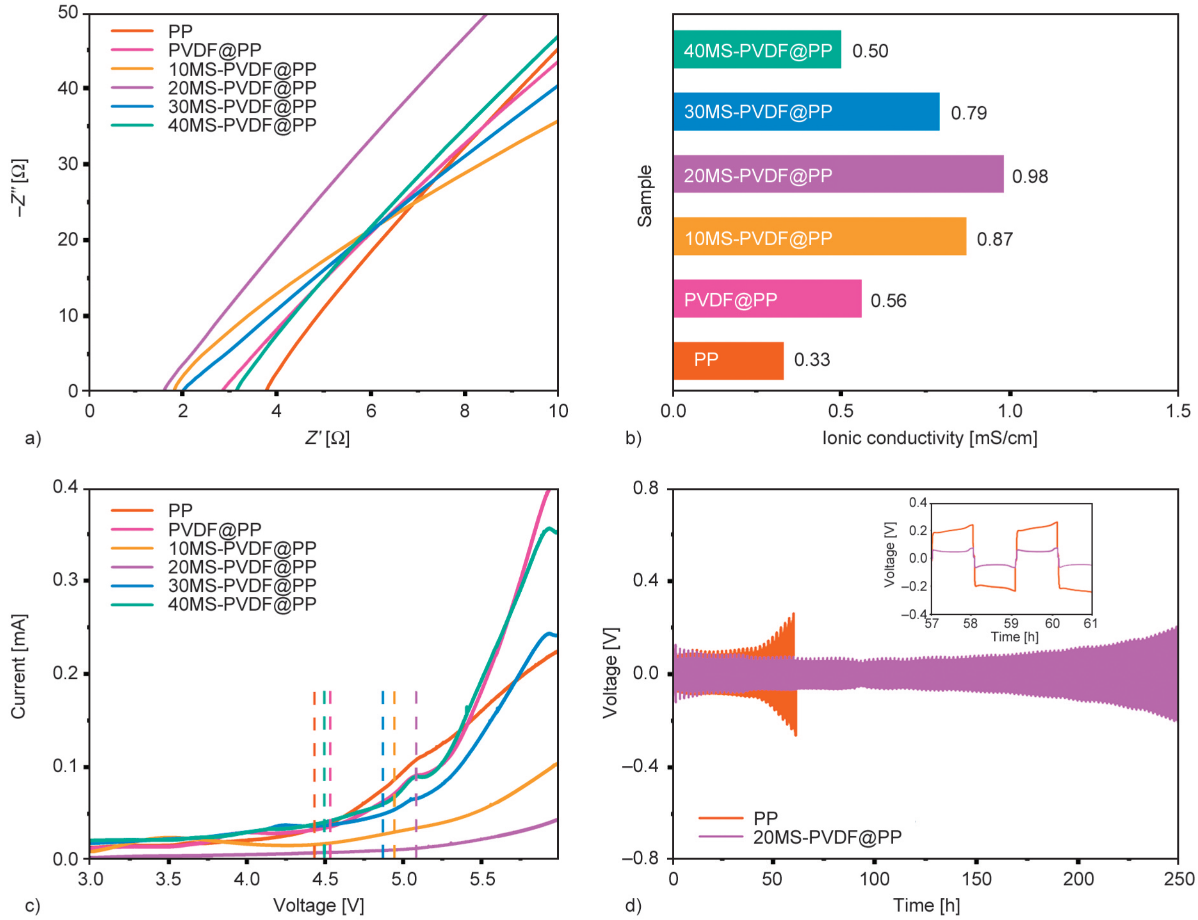

Figure 5. AC impedance spectra (a), ionic conductivity (b) for SS|separator|SS block cells using PP and composite separators, LSV curves for Li|separator|SS cells using PP and composite separators (c), and galvanostatic plating/stripping curves for Li|separator|Li symmetric cells using PP and composite separators at current density and capacity of 1 mA·cm^{-2} and 1 mAh·cm^{-2}, respectively (d).

The electrochemical stability of liquid electrolyte-soaked separators was evaluated by linear sweep voltammetry (LSV). With the increase in voltage, the current increases suddenly at a certain voltage, and the inflection point of the curve corresponds to the decomposition voltage of the electrolyte. Figure 5c shows LSV curves of Li|Separator|SS cells using PP and composite separators. It can be seen that the electrolyte decomposition voltage of composite separators is higher than that of PP separators, indicating that the composite separator has higher electrochemical stability. This can be ascribed to the excellent affinity to liquid electrolytes and properly secured ionic-conducting channels, which are the result of good swelling ability originating from higher specific surface area and porous structure [31]. In addition, the abundant Lewis acid sites on sepiolite surface can interact with PF6- anions (Lewis base) and then retard the decomposition of lithium salt anions [32], thereby further enhancing the electrochemical stability of composite separators.

Li||Li symmetric cells based on PP and 20MS-PVDF@PP separators were assembled to evaluate their performance in the interfacial stability of Li metal anode. Figure 5d shows the plots of voltage *vs*. time at current density and capacity of 1 mA·cm^{-2} and 1 mAh·cm^{-2}, respectively. It can be seen that the Li|PP|Li cell displays higher voltage hysteresis than the Li|20MS-PVDF@PP|Li cell at any time. What's more, the voltage hysteresis of Li|PP|Li cell shows a sudden increment after ~50 h, implying unstable interfacial behavior on the lithium anode surface. It has been reported that all Li$^+$ ions passing through the PP separator tend to aggregate near the pores due to the ionically insulating skeleton. Thereby, the migration of Li$^+$ ions may be impeded by the free anions moving in the opposite direction, which further exacerbates the uneven Li$^+$ ions flux, thus resulting in the growth of lithium dendrites and, finally, a short circuit of the cell [33]. In comparison, the prominent increment of voltage hysteresis happens after ~180 h in Li|20MS-PVDF@PP|Li cell, suggesting the relatively stable lithium plating/stripping behavior and the formation of a stable interfacial layer on the lithium anode surface.

The voltage-time curves of both symmetric cells at 57–61 h are shown in the inset of Figure 5d. It is noticed that Li|20MS-PVDF@PP|Li cell exhibits smaller overpotential, implying better lithium plating/stripping stability. This can be mainly attributed to the higher ionic conductivity of the 20MS-PVDF@PP separator as well as the capture of PF_6^- anions by sepiolite, which facilitates the uniform distribution and deposition of Li$^+$ ions, thereby reducing the probability of lithium dendrite growth. The anion capture capability can be attributed to the Lewis acid-base interaction between sepiolite and PF_6^- [32]. The extended cycle life and stable plating/stripping potential demonstrate that our strategy is effective in constructing a stable interfacial layer on the lithium anode surface.

Figure 6 shows chronoamperometric curves and AC impedance spectra before and polarization for Li||Li symmetric cells using different separators. The Li$^+$ ion transfer number (t_{Li^+}) of different separators can be calculated according to Equation (4), and the obtained t_{Li^+} values are 0.305, 0.488, 0.663, 0.679, 0.612 and 0.397 for PP, PVDF@PP, 10MS-PVDF@PP, 20MS-PVDF@PP, 30MS-PVDF@PP and 40MS-PVDF@PP, respectively. The pore structure and surface characteristics of the separator are the main factors affecting Li$^+$ ion transfer number [34, 35]. The significantly enhanced porosity and electrolyte wettability are conductive to Li$^+$ ions transfer of composite separator. In addition, based on Lewis acid-base interaction, the effectively immobilization of PF_6^- anions by sepiolite can further enhance the Li$^+$ ion transfer number of composite separator. Among them, 20MS-PVDF@PP separator exhibits the highest t_{Li^+} value due to the highest porosity and electrolyte uptake. However, when the addition amount of M-Sep reaches 40 wt%, the Li$^+$ ion transfer number is reduced again, which is related to larger electrospun fiber diameter with nonuniform distribution and the agglomeration of sepiolite. As we know, the electrospun fibers with a larger diameter and nonuniform distribution may block the micropores of the PP separator to a certain extent, and the agglomeration of sepiolite may affect the electrolyte wettability of the separator. Both factors lead to the decrease in porosity and electrolyte uptake and then the decrease in Li$^+$ ions transfer number of separators.

3.3. Cell performance

Li|LiFePO$_4$ CR2430 coin cells using different separators were assembled using PP and xMS-PVDF@PP as separators to investigate their application in LIB. Figure 7a shows the rate performance of Li|LiFePO$_4$ batteries using different separators at 0.5C, 1C, 2C,

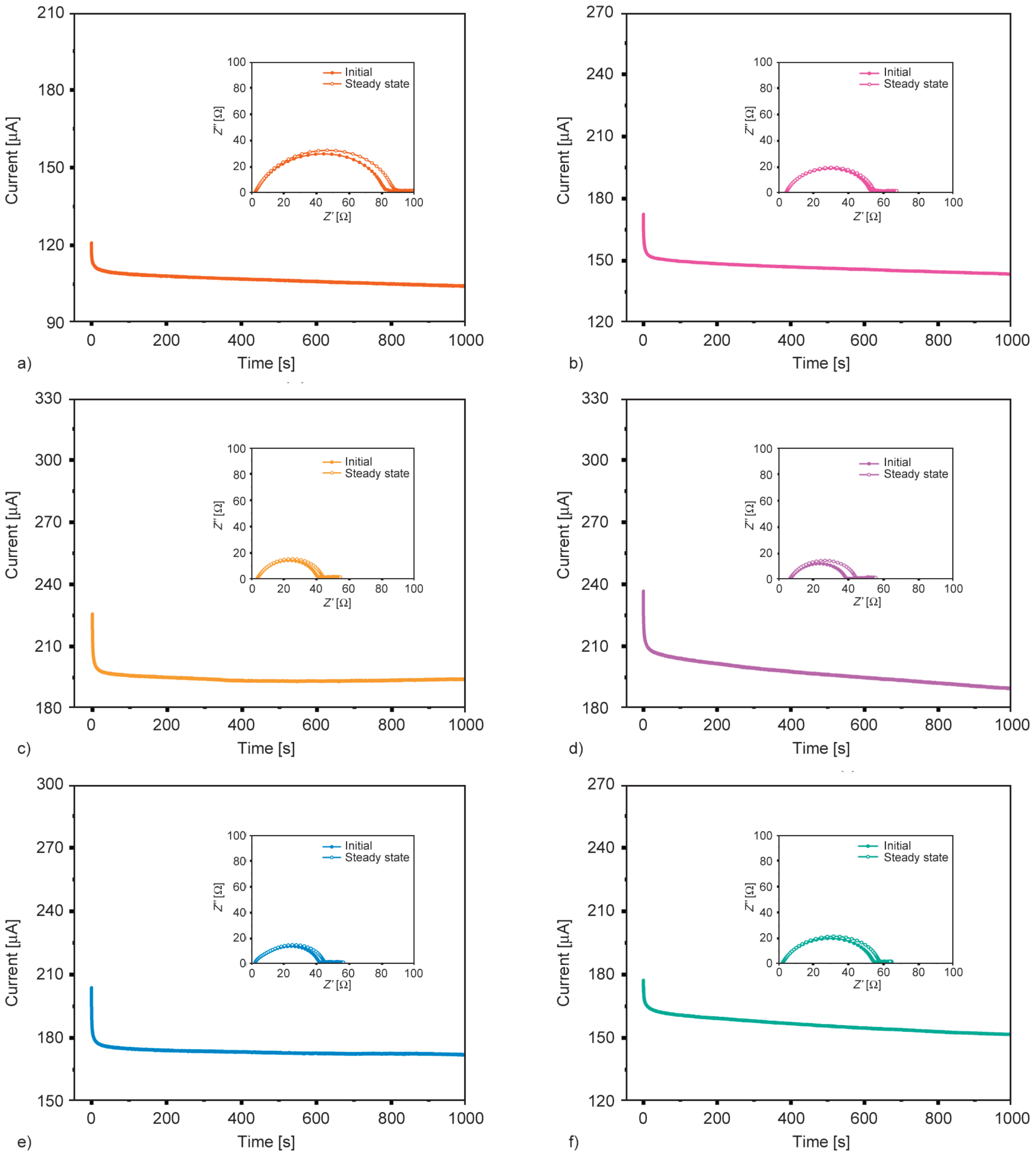

Figure 6. Chronoamperometric curves of Li||Li symmetric cells using PP (a), PVDF@PP (b), 10MS-PVDF@PP (c), 20MS-PVDF@PP (d), 30MS-PVDF@PP (e), 40MS-PVDF@PP (f), and the insets are the corresponding AC impedance spectra before and after polarization.

5C, and 10C rates. It can be seen that the gap between specific discharge capacities of different batteries becomes larger with the increase of current density. Especially, at a high rate of 10C, the specific discharge capacities of Li|$LiFePO_4$ batteries using PP, PVDF@PP, 10MS-PVDF@PP, 20MS-PVDF@PP, 30MS-PVDF@PP and 40MS-PVDF@PP separators are 101.3, 106.2, 113.6, 115.3, 111.5, 102.5 mAh·g^{-1}, respectively. The better rate capability of the batteries using composite separators can be attributed to higher ionic conductivity and Li^+ ion transfer number induced by higher porosity and electrolyte wettability. The poor rate performance of the battery with PP separator can be ascribed to the sluggish Li^+ ion transfer resulting from low porosity and inferior electrolyte wettability of PP separator.

Figure 7b shows the cycling performance curves of Li|$LiFePO_4$ batteries using PP and composite separators at 1C and 25 °C. It is observed that the specific discharge capacities of all batteries gradually increase in initial several cycles, which is called electrochemical activation. The capacity retention rates

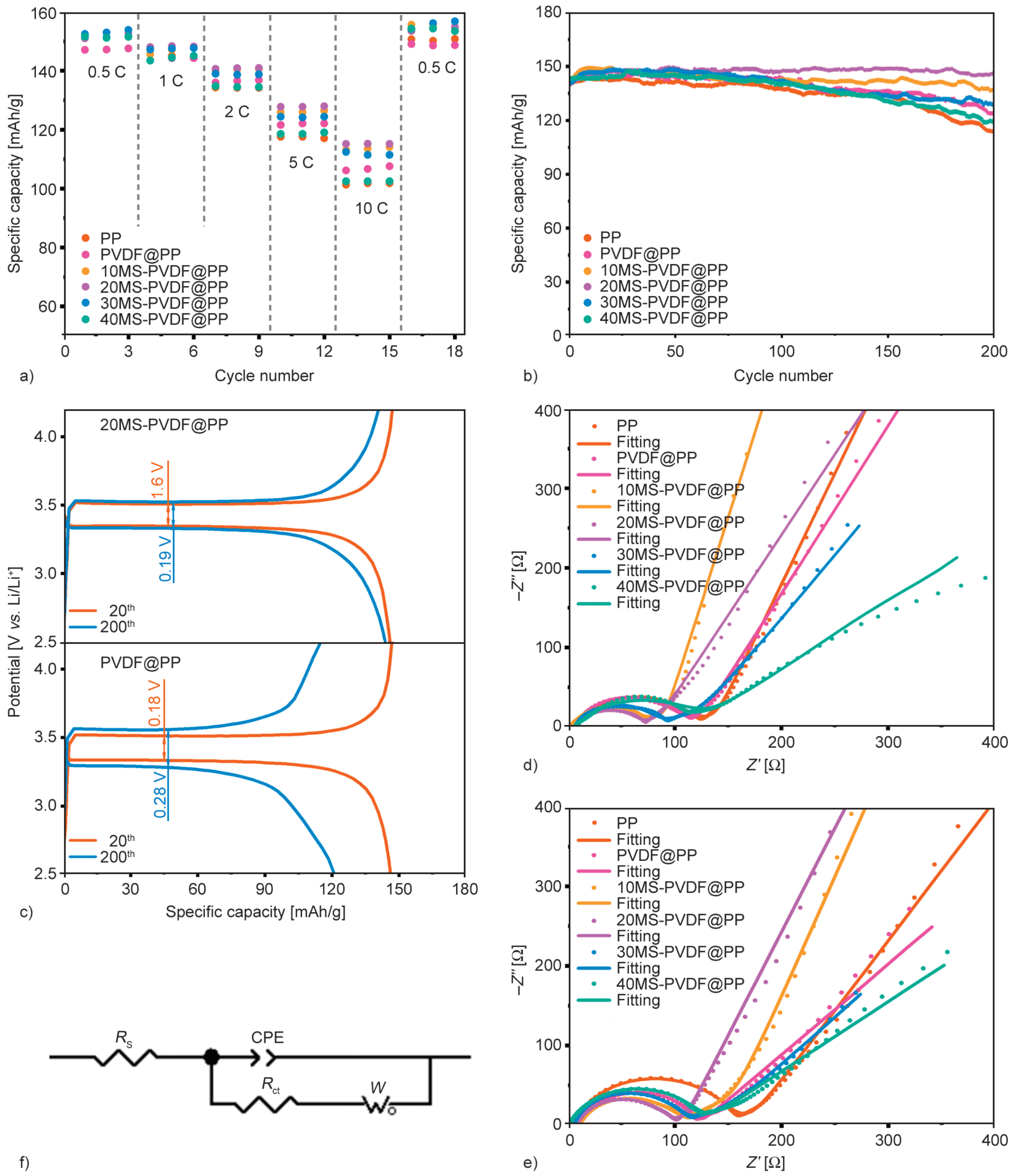

Figure 7. Rate performance curves (a), cycling performance curves (b), charge/discharge curves at 20th and 200th cycles (c), Nyquist plots after 100 and 200 cycles (d, e), and corresponding equivalent circuit (f) for Li|$LiFePO_4$ cells using different separators.

of the batteries using PP, PVDF@PP, 10MS-PVDF@PP, 20MS-PVDF@PP, 30MS-PVDF@PP and 40MS-PVDF@PP separators after 200 cycles are 79.48, 83.71, 91.56, 97.06, 87.04 and 80.75%, respectively. The enhanced cycling performance of the batteries using composite separators can be ascribed to the higher porosity and electrolyte wettability of composite separators, which ensures sufficient participation of Li^+ ions in redox reactions during cycling [36]. In addition, the formation of lithium dendrites on anode surface has been reported to have an influence on the cycling stability of battery [37], because the lithium dendrites growth may consume more organic electrolyte and lithium salt, thereby adversely affecting the Coulombic efficiency and cycling performance of battery. Therefore, the high ionic conductivity and Li^+ ion transfer number of composite separators contribute to the uniform distribution of Li^+ ions, thus inhibiting the growth of lithium dendrites on the anode surface [38]. Besides, the sepiolite nanofibers in an electrospun layer can effectively fix PF_6^- anions based on Lewis acid-base interaction, which is also advantageous to the uniform redistribution of Li^+ ions, thus further improving the cycling performance of $LiFePO_4$ battery.

Figure 7c shows the charge/discharge curves of Li|$LiFePO_4$ cells using PVDF@PP and 20MS-PVDF@PP separators at the 20th and 200th cycles. The difference between the charge and discharge plateaus represents the electrode polarization (ΔV). From the figure, we can see that ΔV values at the 20th and 200th cycles are 0.16, 0.19 V and 0.18, 0.28 V for Li|$LiFePO_4$ cells using PVDF@PP and 20MS-PVDF@PP separators, respectively, that is, the Li|$LiFePO_4$ cell using 20MS-PVDF@PP separator exhibits lower electrode polarization during cycle process. This can be mainly attributed to the higher ionic conductivity and Li^+ ion transfer number induced by higher porosity and electrolyte wettability, as well as the immobilization of PF6- anions by sepiolite.

In order to better understand the impact of electrospun coating on interfacial properties, the AC impedance measurement was carried out on Li|$LiFePO_4$ batteries using different separators after 100 and 200 cycles, as shown in Figures 7d, 7e. All Nyquist plots are composed of a semicircle and a sloping line. The semicircle at the high-frequency region corresponds to charge-transfer resistance at the electrode/electrolyte interface (R_{ct}), and the sloping line in the low-frequency region corresponds to Warburg resistance (Z_w) related to Li^+ ion diffusion in the bulk of electrode material. The plots were fitted via ZView software according to the equivalent circuit in Figure 7f, and the fitted R_{ct} values are shown in Table 2. It is noticed that the R_{ct} values of all batteries using different separators increase with cycle number, whereas the batteries using xMS-PVDF@PP separators show lower R_{ct} values than those using PP and PVDF@PP separators after 100 and 200 cycles. Among them, the battery using 20MS-PVDF@PP separator displays the lowest R_{ct} values during cycle process, which are 56.57 and 84.86 Ω after 100 and 200 cycles, respectively. This can be attributed to the higher ionic conductivity and Li^+ ion transfer number of composite separator as well as the immobilization of PF_6^- anions by sepiolite, which facilitates the uniform distribution of Li^+ ions and then inhibits the growth of lithium dendrites, thereby enhancing the interface stability.

Table 2. Fitted R_{ct} values based on Figures 7d, 7e.

Separator	R_{ct} after 100 cycles [Ω]	R_{ct} after 200 cycles [Ω]
PP	107.00	143.00
PVDF@PP	93.86	113.30
10MS-PVDF@PP	67.71	90.85
20MS-PVDF@PP	56.57	84.86
30MS-PVDF@PP	74.71	94.35
40MS-PVDF@PP	101.20	123.20

3.4. Post-mortem analysis

Figure 8a–8d show SEM images of $LiFePO_4$ cathodes disassembled from Li|$LiFePO_4$ batteries using different separators after 200 cycles. From Figure 8a we can observe the appearance of microcracks (marked with a rectangle) on the surface of $LiFePO_4$ particles from the battery using PVDF@PP separator, and the generation of microcracks is generally induced by HF corrosion. The microcracks can increase the contact area with electrolyte, which can exacerbate the side reactions and lead to the continuous consumption of active lithium, thus resulting in a decline in electrochemical performance. From Figure 8b, 8c, it can be seen that the surface of $LiFePO_4$ particles from the batteries using 10MS-PVDF@PP and 20MS-PVDF@PP separators remains relatively intact without microcracks. This is mainly ascribed to the capability of sepiolite nanofibers to absorb HF, thus reducing damage to cathode material and electrode/electrolyte interface. However, when too much M-Sep is added, the agglomeration of sepiolite nanofibers may reduce its capability to absorb HF, which leads to the appearance of microcracks on the surface of $LiFePO_4$ particles from the battery using 40MS-PVDF@PP separator, as shown in Figure 8d.

Figure 8e–8h shows SEM images of lithium anodes disassembled from Li|$LiFePO_4$ batteries using different separators after 200 cycles. From Figure 8e, some protruding lithium dendrites are observed on the surface of the lithium anode from the battery using the PVDF@PP separator, whereas the surface of lithium anodes from the batteries using 10MS-PVDF@PP and 20MS-PVDF@PP separators is relatively smooth, as shown in Figures 8f, 8g. This is mainly ascribed to the higher ionic conductivity and Li^+ ion transfer number of 10MS-PVDF@PP and 20MS-PVDF@PP separators, as well as the immobilization of PF_6^- anions by the embedded sepiolite

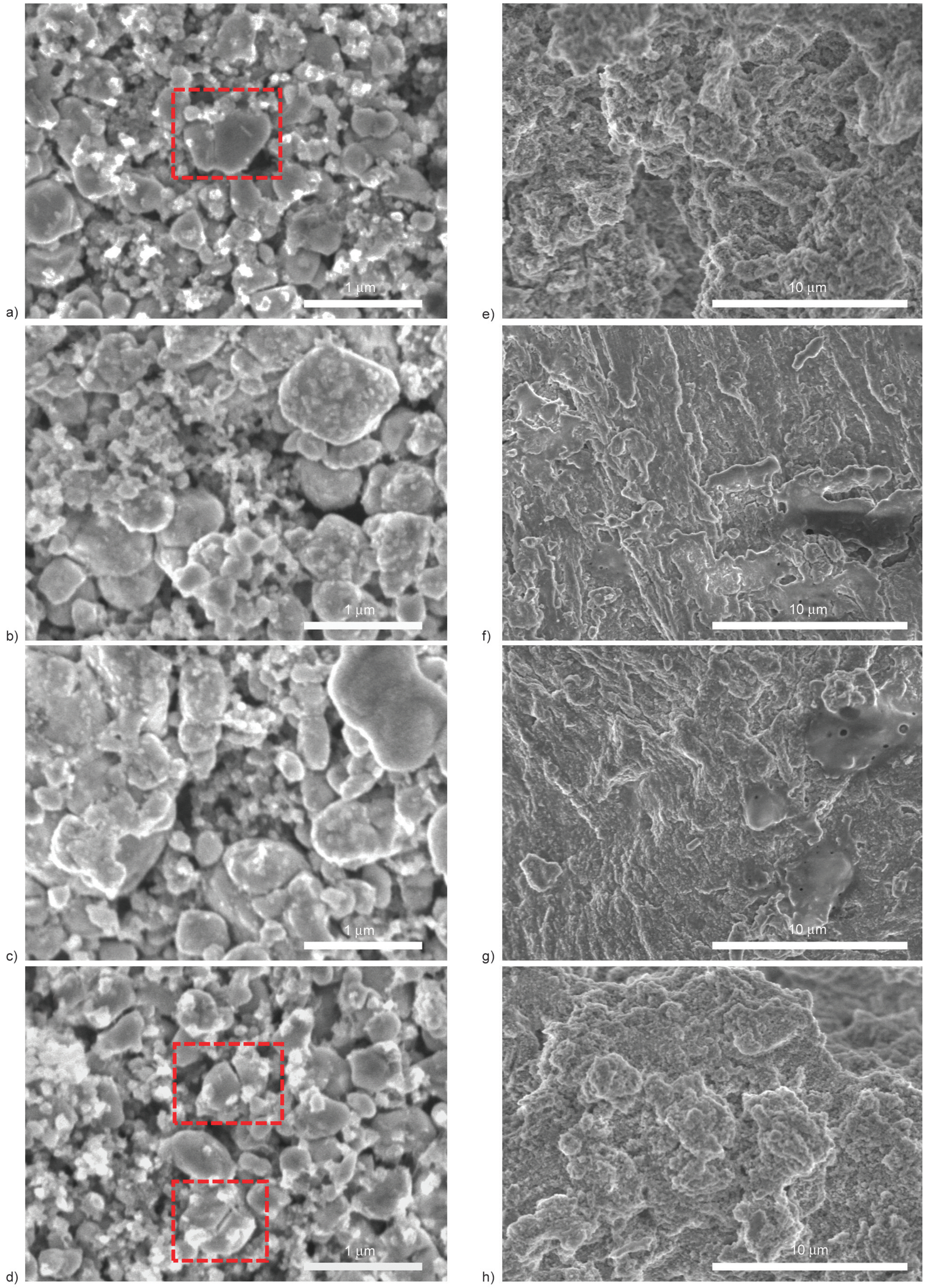

Figure 8. SEM images of $LiFePO_4$ cathodes from Li|$LiFePO_4$ batteries after 200 cycles using different separators: PVDF@PP (a), 10MS-PVDF@PP (b), 20MS-PVDF@PP (c), 40MS-PVDF@PP (d), and SEM images of lithium anodes from Li|$LiFePO_4$ batteries after 200 cycles using different separators: PVDF@PP (e), 10MS-PVDF@PP (f), 20MS-PVDF@PP (g), 40MS-PVDF@PP (h).

nanofibers, which can effectively redistribute Li^+ ions flux evenly, thereby minimizing the growth of lithium dendrite. However, when the additional amount of M-Sep further increases to 40 wt%, more lithium dendrites appear on the surface of the lithium anode from the battery containing 40MS-PVDF@PP, as shown in Figure 8h, which is mainly attributed to the agglomeration of sepiolite nanofibers and the inhomogeneous electrospun fiber morphology. Lithium dendrites will destroy the preformed SEI layer, and new SEI layers are continuously generated by consuming more electrolytes during cycling [39] ultimately the SEI layer is so thick that it affects the transport of Li^+ ions and deteriorates the electrochemical performance of the battery.

Based on the above discussion, it can be concluded that VTES modification can ameliorate the dispersibility of sepiolite nanofibers and their compatibility with the PVDF matrix. The sepiolite-added PVDF coating via electrospinning technology is advantageous to the physical and electrochemical properties of PP separator. Among the composite separators with different amounts of M-Sep, 20MS-PVDF@PP separator shows the best physical and electrochemical properties. The underlying mechanism is illustrated in Figure 9. On the one hand, as for the PP separator, Li^+ ions are mostly huddled in the pores of the PP separator, and PF_6^- anions moving in the opposite direction can obstruct the transport of Li^+ ions, thus leading to the inhomogeneous distribution of Li^+ ions and the formation of lithium dendrite. However, the enhanced porosity, wettability and electrolyte uptake offered by the electrospun layer and the anions immobilization by sepiolite can facilitate the migration of Li^+ ions, which is beneficial to the uniform distribution of Li^+ ions and then inhibits the formation of lithium dendrite. On the other hand, sepiolite nanofibers can scavenge the harmful HF species, which can prevent its corrosion on cathode material and electrode/electrolyte interface, thereby improving the cycling performance of the $LiFePO_4$ battery. In conclusion, the addition of VTES-modified sepiolite offers a multifunctional approach to improve the physical and electrochemical performances of the separator.

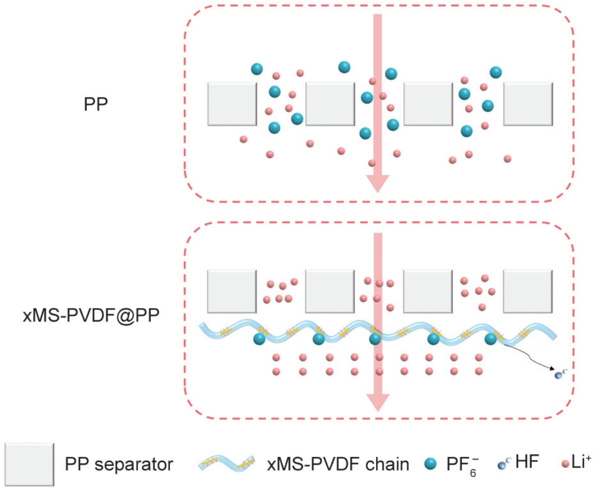

Figure 9. Schematic illustration of reinforcement mechanism of xMS-PVDF@PP composite separator.

4. Conclusions

In summary, electrospinning technology was adopted to prepare a PVDF/sepiolite electrospun coating on one side of the PP separator, in which the sepiolite was modified by VTES to improve its dispersibility and compatibility with the PVDF matrix. The effect of different addition amounts of M-Sep on the physical and electrochemical properties of composite separators was studied. The results show that the addition of M-Sep increases the thermal stability and electrolyte wettability of composite separators. The 20MS-PVDF@PP composite separator with M-Sep addition amount of 20 wt% exhibits the optimal physical and electrochemical properties, with the highest porosity (62%), electrolyte uptake (653%), ionic conductivity ($0.98\ mS\cdot cm^{-1}$) and Li^+ ion transfer number (0.679). In terms of electrochemical performance, $Li|LiFePO_4$ battery using 20MS-PVDF@PP separator demonstrates superior rate capability and cycling stability, with specific discharge capacity of $115.3\ mAh\cdot g^{-1}$ at 10C rate and capacity retention rate of 97.06% after 200 cycles at 1C rate. Besides, the $Li|LiFePO_4$ battery using a 20MS-PVDF@PP separator exhibits smaller electrode polarization during the cycle process. Our study demonstrates that the sepiolite-added PVDF coating via electrospinning technology is an effective means to improve the physical and electrochemical properties of polyolefin separators.

Acknowledgements

This work was supported by the National Natural Science Foundation of China (grant number 51802074).

References

[1] Tarascon J. M., Armand M.: Issues and challenges facing rechargeable lithium batteries. Nature, **414**, 359–367 (2001).
https://doi.org/10.1038/35104644

[2] Scrosati B., Garche J.: Lithium batteries: Status, prospects and future. Journal of Power Sources, **195**, 2419–2430 (2010).
https://doi.org/10.1016/j.jpowsour.2009.11.048

[3] Cheng F., Liang J., Tao Z., Chen J.: Functional materials for rechargeable batteries. Advanced Materials, **23**, 1695–1715 (2011).
https://doi.org/10.1002/adma.201003587

[4] Deimede V., Elmasides C.: Separators for lithium-ion batteries: A review on the production processes and recent developments. Energy Technology, **3**, 453–468 (2015).
https://doi.org/10.1002/ente.201402215

[5] Xiang Y., Li J., Lei J., Liu D., Xie Z., Qu D., Li K., Deng T., Tang H.: Advanced separators for lithium-ion and lithium-sulfur batteries: A review of recent progress. ChemSusChem, **9**, 3023–3039 (2016).
https://doi.org/10.1002/cssc.201600943

[6] Peng L., Shen X., Dai J., Wang X., Zeng J., Huang B., Li H., Zhang P., Zhao J.: Three-dimensional coating layer modified polyolefin ceramic-coated separators to enhance the safety performance of lithium-ion batteries. Journal of the Electrochemical Society, **166**, A2111–A2120 (2019).
https://doi.org/10.1149/2.1141910jes

[7] Zhao P., Yang J., Shang Y., Wang L., Fang M., Wang J., He X.: Surface modification of polyolefin separators for lithium ion batteries to reduce thermal shrinkage without thickness increase. Journal of Energy Chemistry, **24**, 138–144 (2015).
https://doi.org/10.1016/S2095-4956(15)60294-7

[8] Huang X.: Performance evaluation of a non-woven lithium ion battery separator prepared through a paper-making process. Journal of Power Sources, **256**, 96–101 (2014).
https://doi.org/10.1016/j.jpowsour.2014.01.080

[9] Li T., Panda P. K., Hsieh C-T., Gandomi Y. A., Yang P-C.: Lithium iron phosphate cathode supported solid lithium batteries with dual composite solid electrolytes enabling high energy density and stable cyclability. Journal of Energy Storage, **81**, 110444 (2024).
https://doi.org/10.1016/j.est.2024.110444

[10] Luiso S., Henry J. J., Pourdeyhimi B., Fedkiw P. S.: Fabrication and characterization of meltblown poly (vinylidene difluoride) membranes. ACS Applied Polymer Materials, **2**, 2849–2857 (2020).
https://doi.org/10.1021/acsapm.0c00395

[11] Alcoutlabi M., Lee H., Watson J. V., Zhang X.: Preparation and properties of nanofiber-coated composite membranes as battery separators *via* electrospinning. Journal of Materials Science, **48**, 2690–2700 (2013).
https://doi.org/10.1007/s10853-012-7064-0

[12] Jung J-W., Lee C-L., Yu S., Kim I-D.: Electrospun nanofibers as a platform for advanced secondary batteries: A comprehensive review. Journal of Materials Chemistry A, **4**, 703 (2016).
https://doi.org/10.1039/c5ta06844d

[13] Yang Y., Yang B., Luo M., Yang Y., Wang Y., Miao J., Wang S., Zheng Z., Qian J., Xia R., Ke Y., Tu Y.: Considerably enhanced electrochemical and thermomechanical performance of lithium battery (LIB) separators of PVDF/vermiculite nanosheets (VNs) composites via constructing well-defined hierarchical microstructure. Electrochimica Acta, **446**, 142074 (2023).
https://doi.org/10.1016/j.electacta.2023.142074

[14] Liu T., Hu X., Zhang Y., He T., Zhou J., Qiao J.: Ion transport regulated lithium metal batteries achieved by electrospun ZIF/PAN composite separator with suitable electrolyte wettability. Batteries, **9**, 166 (2023).
https://doi.org/10.3390/batteries9030166

[15] Deng C., Jiang Y., Fan Z., Zhao S., Ouyang D., Tan J., Zhang P., Ding Y.: Sepiolite-based separator for advanced Li-ion batteries. Applied Surface Science, **484**, 446–452 (2019).
https://doi.org/10.1016/j.apsusc.2019.04.141

[16] Guo J., Zhang Y., Fu S., Yan S., Lang Y., Wang L., Liang G.: Sepiolite-assisted separator modification process for high-voltage $LiNi_{0.5}Mn_{1.5}O_4$ batteries and the influence on electrodes. Industrial and Engineering Chemistry Research, **60**, 11117–11127 (2021).
https://doi.org/10.1021/acs.iecr.1c01685

[17] Zhang Y., Mei Y., Pang Y., Xiao Y., Tang Z., Gao X., Deng J.: Excellent high-temperature resistance performance of one-dimensional sepiolite coated membrane based on an organic-inorganic composite binder for lithium ionic batteries. Journal of Power Sources, **584**, 233601 (2023).
https://doi.org/10.1016/j.jpowsour.2023.233601

[18] Wang Y., Tang Z., Chen M., Zhang J., Shi J., Wang C., Yang Z., Wang J.: Effect of Mo content in Mo/Sepiolite catalyst on catalytic depolymerization of Kraft lignin under supercritical ethanol. Energy Conversion and Management, **222**, 113227 (2020).
https://doi.org/10.1016/j.enconman.2020.113227

[19] Kim J-S., Choi M-C., Jeong K-M., Kim G-H., Ha C-S.: Enhanced interaction in the polyimide/sepiolite hybrid films via acid activating and polydopamine coating of sepiolite. Polymers for Advanced Technologies, **29**, 1404–1413 (2018).
https://doi.org/10.1002/pat.4252

[20] Shafiq M., Yasin T., Saeed S.: Synthesis and characterization of linear low-density polyethylene/sepiolite nanocomposites. Journal of Applied Polymer Science, **123**, 1718–1723 (2012).
https://doi.org/10.1002/app.34633

[21] Ruiz-Hitzky E.: Molecular access to intracrystalline tunnels of sepiolite. Journal of Materials Chemistry, **11**, 86 (2001).
https://doi.org/10.1039/b003197f

[22] Karatas D., Arslan D. S., Unver I. K., Ozdemir O.: Coating mechanism of AuNPs onto sepiolite by experimental research and MD simulation. Coatings, **9**, 785 (2019). https://doi.org/10.3390/coatings9120785

[23] Zhang X., Lin W., Zheng J., Sun Y., Xia B., Yan L., Jiang B.: Insight into the organic-inorganic hybrid and microstructure tailor mechanism of sol-gel ORMOSIL antireflective coatings. The Journal of Physical Chemistry C, **122**, 596–603 (2018). https://doi.org/10.1021/acs.jpcc.7b10294

[24] Mohammadzad M. K., Pircheraghi G., Sharifi H.: Fabrication, characterization, and electrochemical performance of the HDPE/sepiolite nanocomposite as a novel separator for Li-ion batteries. Express Polymer Letters, **15**, 1063–1080 (2021). https://doi.org/10.3144/expresspolymlett.2021.86

[25] Liu J., He C., He J., Cui J., Liu H., Wu X.: An enhanced poly(vinylidene fluoride) matrix separator with high density polyethylene for good performance lithium ion batteries. Journal of Solid State Electrochemistry, **21**, 919–925 (2017). https://doi.org/10.1007/s10008-016-3444-8

[26] Kang W., Ma X., Zhao H., Ju J., Zhao Y., Yan J., Cheng B.: Electrospun cellulose acetate/poly(vinylidene fluoride) nanofibrous membrane for polymer lithium-ion batteries. Journal of Solid State Electrochemistry, **20**, 2791–2803 (2016). https://doi.org/10.1007/s10008-016-3271-y

[27] Mao Y., Sun W., Qiao Y., Liu X., Xu C., Fang L., Hou W., Wang Z., Sun K.: A high strength hybrid separator with fast ionic conductor for dendrite-free lithium metal batteries. Chemical Engineering Journal, **416**, 129119 (2021). https://doi.org/10.1016/j.cej.2021.129119

[28] Hao X., Zhu J., Jiang X., Wu H., Qiao J., Sun W., Wang Z., Sun K.: Ultrastrong polyoxyzole nanofiber membranes for dendrite-proof and heat-resistant battery separators. Nano Letters, **16**, 2981–2987 (2016). https://doi.org/10.1021/acs.nanolett.5b05133

[29] Chen H., Zheng M., Sun H., Jia Q.: Characterization and properties of sepiolite/polyurethane nanocomposites. Materials Science and Engineering: A, **445–446**, 725–730 (2007). https://doi.org/10.1016/j.msea.2006.10.008

[30] Ulaganathan M., Lei Y. L., Flora X. H., Yan Q.: Charge transport, mechanical and storage performances of sepiolite based composite polymer electrolytes. ChemistrySelect, **1**, 5821–5827 (2016). https://doi.org/10.1002/slct.201601121

[31] Jung H-R., Ju D-H., Lee W-J., Zhang X., Kotek R.: Electrospun hydrophilic fumed silica/polyacrylonitrile nanofiber-based composite electrolyte membranes. Electrochimica Acta, **54**, 3630–3637 (2009). https://doi.org/10.1016/j.electacta.2009.01.039

[32] Fang C., Yang S., Zhao X., Du P., Xiong J.: Electrospun montmorillonite modified poly(vinylidene fluoride) nanocomposite separators for lithium-ion batteries. Materials Research Bulletin, **79**, 1–7 (2016). https://doi.org/10.1016/j.materresbull.2016.02.015

[33] Huo H., Li X., Chen Y., Liang J., Deng S., Gao X., Doyle-Davis K., Li R., Guo X., Shen Y., Nan C-W., Sun X.: Bifunctional composite separator with a solid-state-battery strategy for dendrite-free lithium metal batteries. Energy Storage Materials, **29**, 361–366 (2020). https://doi.org/10.1016/j.ensm.2019.12.022

[34] Lagadec M. F., Zahn R., Wood V.: Characterization and performance evaluation of lithium-ion battery separators. Nature Energy, **4**, 16–25 (2019). https://doi.org/10.1038/s41560-018-0295-9

[35] Wang Z., Guo F., Chen C., Shi L., Yuan S., Sun L., Zhu J.: Self-assembly of PEI/SiO_2 on polyethelene separators for Li-ion batteries with enhanced rate capability. ACS Applied Materials and Interfaces, **7**, 3314–3322 (2015). https://doi.org/10.1021/am508149n

[36] Zhong S., Yuan B., Guang Z., Chen D., Li Q., Dong L., Ji Y., Dong Y., Han J., He W.: Recent progress in thin separators for upgraded lithium ion batteries. Energy Storage Materials, **41**, 805–841 (2021). https://doi.org/10.1016/j.ensm.2021.07.028

[37] Wang C., Zhu G., Hu Y., Sun J., Xu J., Wang L., Wang H., Cheng C.: Ionic conductivity and cycling stability-enhanced composite separator using hollow halloysite nanotubes constructed on PP nonwoven through polydopamine-induced water-based coating method. Colloids and Surfaces A: Physicochemical and Engineering Aspects, **667**, 131403 (2023). https://doi.org/10.1016/j.colsurfa.2023.131403

[38] Wang W., Yuen A. C. Y., Yuan Y., Liao C., Li A., Kabir I. I., Kan Y., Hu Y., Yeoh G. H.: Nano architectured halloysite nanotubes enable advanced composite separator for safe lithium metal batteries. Chemical Engineering Journal, **451**, 138496 (2023). https://doi.org/10.1016/j.cej.2022.138496

[39] Ryou M-H., Lee D. J., Lee J-N., Lee Y. M., Park J-K., Choi J. W.: Excellent cycle life of lithium-metal anodes in lithium-ion batteries with mussel-inspired polydopamine-coated separators. Advanced Energy Materials, **2**, 645–650 (2012). https://doi.org/10.1002/aenm.201100687